Post-Repolarization Block of Cardiac Sodium Channels by Saxitoxin

Jonathan C. Makielski, Jonathan Satin, and Zheng Fan
Cardiac Electrophysiology Laboratories, University of Chicago, Chicago, Illinois 60637, USA

ABSTRACT Phasic block of rat cardiac Na^+ current by saxitoxin was assessed using pulse trains and two-pulse voltage clamp protocols, and the results were fit to several kinetic models. For brief depolarizations (5 to 50 ms) the depolarization duration did not affect the rate of development or the amplitude of phasic block for pulse trains. The pulse train data were well described by a recurrence relation based upon the guarded receptor model, and it provided rate constants that accurately predicted first-pulse block as well as recovery time constants in response to two-pulse protocols. However, the amplitudes and rates of phasic block development at rapid rates (>5 Hz) were less than the model predicted. For two pulse protocols with a short (10 ms) conditioning step to −30 mV, block developed only after repolarization to −150 mV and then recovered as the interpulse interval was increased. This suggested that phasic block under these conditions was caused by binding with increased affinity to a state that exists transiently after repolarization to −150 mV. This "post-repolarization block" was fit to a three-state model consisting of a transient state with high affinity for the toxin, the toxin bound state, and the ultimate resting state of the channel. This model accounted for the biphasic post-repolarization block development and recovery observed in two-pulse protocols, and it more accurately described phasic block in pulse trains. The transient state after repolarization was predicted to have a dwell time of 570 ms, an on rate for saxitoxin of 16 $s^{-1}\mu M^{-1}$, and an off rate of 0.2 s^{-1} (K_D = 12 nM). These results and the proposed model suggest a novel variation on phasic block mechanisms and suggest a long-lived transient Na^+ channel conformation during recovery.

INTRODUCTION

Phasic or use-dependent block of cardiac Na^+ current (I_{Na}) by tetrodotoxin (TTX) was first described using action potential upstroke velocity as an index of I_{Na} (Baer et al., 1976), and it has subsequently been studied more directly in heart by voltage clamp (e.g., Cohen et al., 1981; Vassilev et al., 1986; Watanabe and McDonald, 1986; Carmeliet, 1987; Clarkson et al., 1988; Eickhorn et al., 1990). Phasic block of I_{Na} was at first thought to be unique to cardiac Na^+ channels, but it has now been described for both TTX and the related saxitoxin (STX) in noncardiac preparations (e.g., Gonoi et al., 1985; Salgado et al., 1986; Lönnendonker, 1989; Patton and Goldin, 1991). Salgado and co-workers (Salgado et al., 1986) reported an intriguing aspect of STX block of Na^+ channels in giant crayfish axons that may be called post-repolarization block. They reported that the additional block that was induced by a brief depolarization occurred not during the depolarization but rather after the membrane was repolarized. This same effect was observed for STX and TTX block of I_{Na} in myelinated nerve (Lönnendonker, 1991), for TTX block of rat brain II Na^+ channels expressed in oocytes (Patton and Goldin, 1991), and for STX block of rat heart I channels expressed in oocytes (Satin et al., 1992b).

Cardiac Na^+ channels are less sensitive to block by STX and TTX than most nerve and skeletal muscle Na^+ channels, and this property has been important in characterizing the binding site for these toxins (Noda et al., 1989; Satin et al., 1992a). TTX and STX share a guanidinium group that is thought to account for their specificity in blocking Na^+ channels at the same site (Ulbricht et al., 1986). The toxins differ in that STX has two net positive charges, whereas TTX has a single net positive charge, and STX has faster binding and unbinding kinetics than TTX (Ulbricht et al., 1986). Phasic block of cardiac I_{Na} by STX has not been previously studied in detail. We propose a quantitative model to explain post-repolarization and phasic block that postulates a high affinity state for STX existing transiently after repolarization. This model represents a novel mechanism for phasic block in that the binding occurs after and not during the depolarization. In addition, the model predicts a long-lived conformation during the recovery process not previously suspected from studies of Na^+ channel gating. Finally, the time course of peak post-repolarization block in heart is more rapid than that reported for non-heart channels, providing a functional difference that might be correlated with structures of Na^+ channel isoforms. Some of these data have been presented previously in abstract form (Fan and Makielski, 1992a,b).

MATERIALS AND METHODS

Preparation and solutions

Single ventricular myocytes from rat hearts were prepared by an enzymatic dissociation procedure. For measuring I_{Na}, the external solution contained (in mM) NaCl, 45; CsCl, 90; $CaCl_2$, 1; $MgCl_2$, 1.2; glucose, 11.0; 4-(2-hydroxyethyl)-1-piperazineethanesulfonic acid, 20.0 (pH 7.4 adjusted by CsOH). The pipette solution contained (in mM) CsF, 140; Na_2ATP, 2.5; EGTA, 5; 4-(2-hydroxyethyl)-1-piperazineethanesulfonic acid, 5.0 (pH 7.3 adjusted with CsOH). The experiments were performed at room temperature (22 to 24°C).

Received for publication 8 January 1993 and in final form 3 May 1993.
Address reprint requests to J. C. Makielski, M.D., University of Chicago Medical Center, 5841 S. Maryland Avenue, MC 6094, Chicago, IL 60637.

0006-3495/93/08/790/09 $2.00

Recording techniques and control currents

I_{Na} was recorded by a whole-cell patch-clamp technique similar to that described previously (Makielski et al., 1987) with the exception that the pipette was not internally perfused. The diameter of the pipette was estimated to be 5–7 μm. Voltage protocols were imposed by a 16-bit DA converter (Masscomp 5450) over a 30/1 voltage divider using locally written control programs (Hanck et al., 1990). The voltage command was then imposed via a unity gain amplifier (Burr-Brown OPA-27, Tucson, AZ) located in the head stage, and I_{Na} was measured with a virtual ground amplifier (Burr-Brown OPA-101). Currents were recorded with a 16-bit AD converter on a Masscomp 5540 computer (Concurrent Computer, Tinto Falls, NJ) at 100 kHz. Data were filtered with an 16-pole Bessel filter (Frequency Devices 9902, Haverhill, MS) with a −3-dB corner frequency of 10 kHz. A fraction of the current was fed back to compensate for the voltage drop across the series resistance (R_s), which was 100–200 kΩ across the open pipette. The characteristics of each cell were assessed in control solutions using protocols for measurement of capacity, peak current voltage relationships, and voltage dependent I_{Na} availability (h_∞ type) as previously described (Makielski et al., 1987). An example of typical control currents is shown in Fig. 1. Adequacy of voltage control during I_{Na} is supported by the graded slope on the negative limb of the peak current-voltage relationship (Fig. 1, *left*) and by the alignment of the peaks of the I_{Na} traces of different amplitudes in the steady-state availability protocol (Fig. 1, *upper right*). Cells were held at −150 mV to assure full I_{Na} availability. In 14 cells the capacity was 133 ± 19 pF, the leak resistance was 40 ± 44 MΩ (minimum 21), the maximal conductance from the peak current-voltage relationship was 0.83 ± 0.3 μS, the peak I_{Na} at −20 mV was −64 ± 25 nA, and the half-point of the I_{Na} availability relationship was −94 ± 4 mV. The primary charging time constant measured before R_s compensation was 60 ± 17 μs and with R_s compensation the capacity current settled to within 0.67 of its final value before 30 μS. Test protocols for STX block consisted of either trains of depolarizations or "two-pulse" recovery type protocols, the details of which are presented with the Results. An interval of at least 30 s at −150 mV was introduced between test protocols in the presence of STX, and this interval was sufficient to allow full recovery from phasic block.

Data analysis

The pulse-by-pulse decline in peak current was fitted to a single exponential model by DISCRETE (Provencher, 1976) using the equation

$$I_n = I_{amp} * e^{-n\lambda} + I_b \quad (1)$$

where I_n (nA) is the peak current measured for the nth depolarization in a train, I_{amp} (nA) is the amplitude of current phasically blocked, I_b (nA) is the final value of peak current at the end of the train, and λ (pulses^{-1}) is the rate of block development per depolarization. The "steady-state" amplitude of the block (a_{ss}, referred to as phasic block) was normalized by

$$a_{ss} = I_{amp}/(I_{amp} + I_b) \quad (2)$$

Results (a_{ss} and λ) from 56 pulse trains at four concentrations of STX at four different frequencies in seven cells were fit to the recurrence relations derived from the guarded receptor model or to the recurrence relations derived from a three-state model (see Appendix).

The data for the two-pulse protocols were normalized by dividing the current in response to the second test depolarization (I_t) by the current in the conditioning depolarization (I_1). This normalization method does not include nonphasic or rest block by STX. When we wished to consider nonphasic block together with phasic block, the data were normalized by dividing I_t by the control current (I_C) in the absence of STX. These data were fit to single- or double-component exponential models as described in the Results using nonlinear regression, and they were fit to a three-state model described in the Appendix. All fitting programs were written in SAS (Cary, NC) using the NLIN nonlinear least-squares fitting procedure with a CONVERGE criteria of 0.0001 running on a Sun Sparcstation SLC.

RESULTS

Nonphasic and phasic block

STX induced both phasic and nonphasic block of I_{Na}. Nonphasic block (often called rest block, tonic block, or first

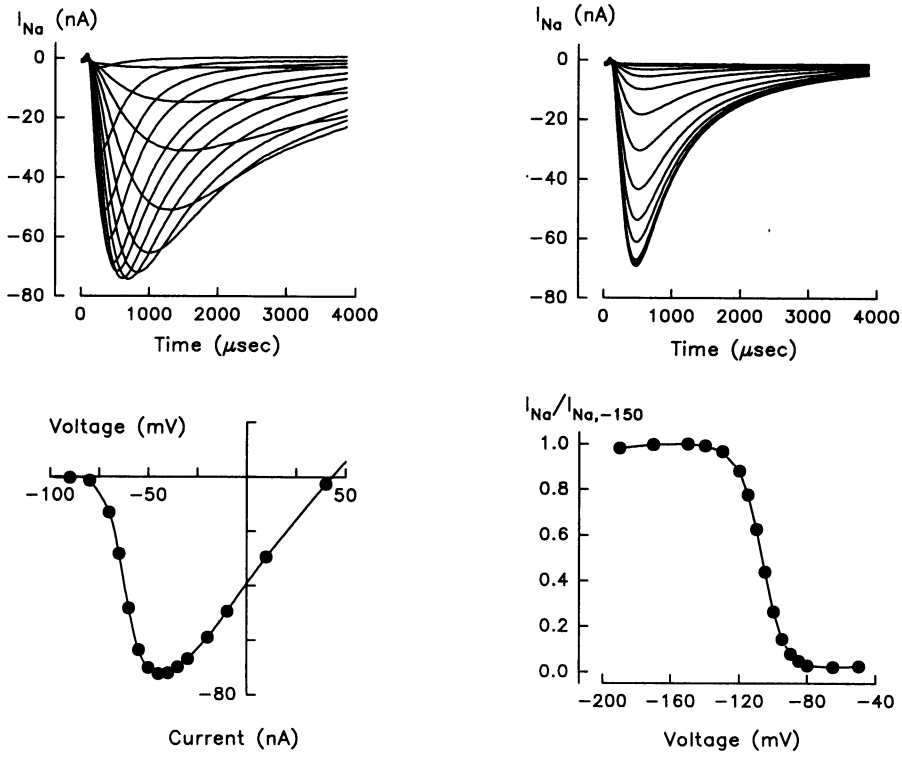

FIGURE 1 Peak current voltage relationship (*left*) and steady-state availability (*right*) for I_{Na} in control solutions. From a holding potential of −150 mV I_{Na} (*traces top left*) was elicited by depolarizations to various potentials. The peak I_{Na} was plotted for each depolarization potential (*bottom left*) and shows a smoothly graded response between −70 mV and −50 mV consistent with adequate voltage control during I_{Na}. The "steady state" voltage-dependent availability for I_{Na} was determined by conditioning for 500 ms at various potentials, followed by a test depolarization to −20 mV (h_∞ type protocol). The currents in response to the test depolarization (*top right*) show that I_{Na} peaked at the same time for different current amplitudes, again an indication of adequate voltage control during I_{Na}. The peak currents for each test depolarization were normalized to the peak current from a holding potential of −150 mV and plotted against the conditioning potential (*bottom right*) to show the dependence of I_{Na} availability on conditioning voltage (fd.28).

pulse block) is evident in Fig. 2*A* as the difference in the control current (labeled *C*) and the first current (labeled *1*) after the addition of 100 nM STX to the bath. For STX, peak I_{Na} always returned to the same level after a 30-s rest. The concentration response relationship for first pulse block was well fit by a single-site binding curve with a K_D of 61 nM (n = 6 cells).

Phasic block (also often called use-dependent block, frequency-dependent block, or extra block) is demonstrated by the I_{Na} response to the 80th depolarization in the train (Fig. 2*A*). A plot of the pulse by pulse measure of peak I_{Na} (Fig. 2*B*) demonstrates the negligible fall of peak I_{Na} in control solutions. First pulse block is evident for the first depolarization in the train after STX was added to the bath, and phasic block is then apparent as an exponential fall in peak I_{Na}. STX was removed from the bath in two cells, and STX block disappeared completely within 2 min. This indicates that rundown of I_{Na} was not a problem during the time course of these experiments and that the holding potential was sufficiently negative that the shift in I_{Na} availability (Makielski et al., 1987) that can occur in whole cell voltage clamp did not affect the interpretation of these results.

Transient state versus maintained state block

One of the first tasks in characterizing phasic block in terms of the modulated receptor model (Courtney, 1975; Hille, 1977; Hondeghem and Katzung, 1977) is to determine whether there is binding to a state maintained throughout the depolarization such as the inactivated state, or whether there is binding only to a transiently available state such as the open state. Maintained state block should depend directly upon the duration of the depolarization because this allows more time for high-affinity binding to occur. For STX block of cardiac I_{Na} in response to pulse trains the amplitude and rate of block were not significantly affected by prolonging the duration of the depolarization from 5 to 50 ms (50 nM STX, n = 5, interpulse intervals of 0.2 and 1.0 s). Therefore, we attributed the predominant phasic block developed during pulse trains with depolarizations of 10-ms duration to a state of the Na^+ channel that is transiently available in association with each depolarization.

Frequency and concentration dependence of phasic block for pulse trains

The amplitude of phasic block was greater at shorter intervals between depolarizations and for larger STX concentrations (Fig. 3*A*). The rate of development of phasic block was more rapid for larger STX concentrations and for longer intervals (Fig. 3*B*). The guarded receptor model (Starmer et al., 1984; Starmer and Grant, 1985), which was developed as a simplification of the modulated-receptor model, allows calculation of apparent binding (on rate) and unbinding (off rate) rates from pulse train data. The apparent on rate and off rate for the resting state of the channel predict equilibrium binding to the resting state of the channel to be 61 nM, which is remarkably close to the single-site binding curve fit of 62 nM. Note that the model prediction (Fig. 3, *dashed lines*) deviates from the data for short interpulse intervals (<0.3 s). To examine this discrepancy we looked at recovery from block induced by pulse trains and by long or short depolarizations.

Recovery from phasic STX block

In control, a conditioning pulse train caused only a small decrease in I_{Na} (Fig. 4*A*), and recovery was rapid (<0.1 s). In 50 nM STX nearly 60% of I_{Na} was blocked by the train, and recovery occurred with a time constant of 4.3 s when fit by a single exponential. The recovery time constant predicted by the guarded receptor model off rate is $1/l_r$ = 5.6 s. Considering that the recovery data were not included in the fit, the two values are similar.

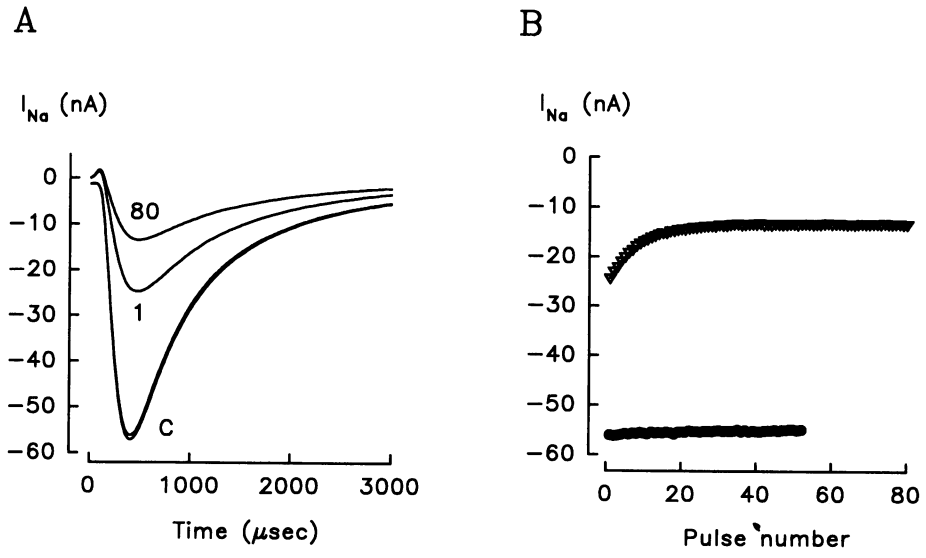

FIGURE 2 (*A*) Superimposed I_{Na} records before and after exposure to 100 nM STX. A train of 80 depolarizing pulses of 10-ms duration was applied from a holding potential of −150 mV to −30 mV at 10 Hz. The I_{Na} records in response to the first (1) and last (80) depolarizations in control solutions (*C*) and in STX are displayed. (*B*) Plot of peak I_{Na} against pulse number in a train of depolarizations under control conditions (●) and in the presence of 100 nM STX (▽). The decline in peak I_{Na} was fit to a single exponential (see Materials and Methods) to obtain the rate (λ) and amplitude of phasic block (fd.21 11&26).

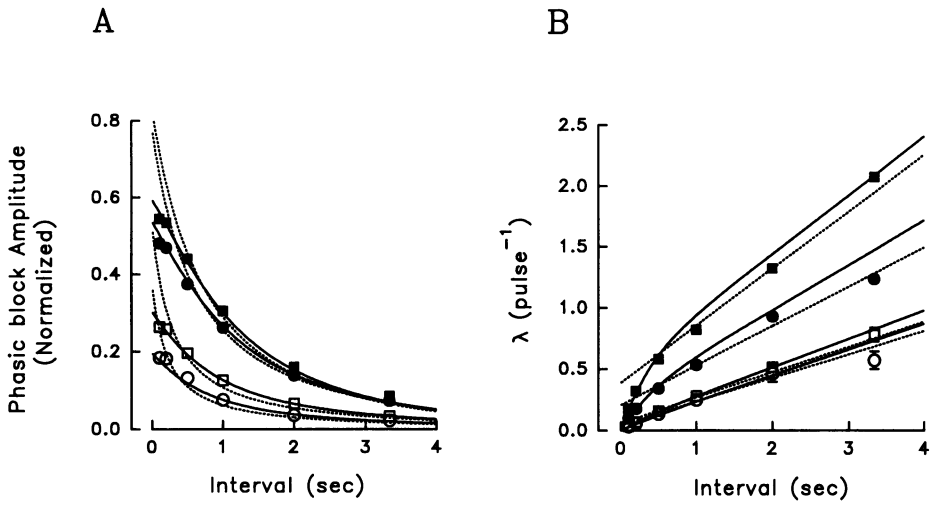

FIGURE 3 Frequency dependence of phasic block at different concentrations of STX. (*A*) Amplitude of steady state phasic block is normalized to the current in the first pulse and plotted against the interpulse interval at STX concentrations: 5 nM (○); 10 nM (□); 50 nM (●); 100 nM (■). (*B*) Rate of development of phasic block (λ) against interpulse interval for different concentrations as in *A*. The symbols represent mean data from 3–6 measurements; SE bars are not shown where they are smaller than the symbol size. The interrupted lines in both panels are a guarded receptor model fit using the equations given in the appendix and the rate constants $k_a = 3.62 \pm 0.12$ nM^{-1}s^{-1}ms^{-1}, $l_a = 24.8 \pm 4.3$ s^{-1}, $k_r = 0.0029 \pm 0.0001$ nM^{-1}s^{-1}, and $l_r = 0.178 \pm 0.005$ s^{-1} (± approximate SE of the parameter fit). The solid lines are from the three-state model for post-repolarization block (Table 1, fit 3). Note how the post-repolarization block model (——) fits the data better than the guarded-receptor model (·····) at short intervals (fd.24, 25, 26, 27, 28, 30).

Recovery from STX block was also evaluated using a single 5-s conditioning pulse in a two-pulse recovery protocol (Fig. 4*B*). In control, peak I_{Na} recovered with a time constant of 0.30 s (amplitude 0.28). In 50 nM STX, I_{Na} was decreased by 36%, and recovery was biexponential (Fig. 4*B*), with the rapid component having a time constant and amplitude similar to that of the recovery in control (0.31 ms and 0.21). The slower time constant (4.88 s; amplitude, 0.17) was similar to that found in the recovery from pulse trains (4.26 s). Rapid recovery from inactivation was presumably complete before 100 ms and was not apparent on this time scale. Recovery in control solutions and the first, more rapid time constant in STX might be attributed to slow recovery from inactivation, and the second, slower time constant in STX to recovery of STX blocked channels. This conditioning protocol confirmed that STX will bind to the Na^+ channel during a prolonged 5-s depolarization, presumably to a maintained inactivated state. STX binding to this inactivated state was not studied further.

Two-pulse recovery protocols were also performed using a single 10-ms duration conditioning pulse (Fig. 4*C*), the same depolarization duration as was used in the pulse trains. In control solutions the 10-ms conditioning depolarization produced a very small (<3%) inactivation of I_{Na} that recovered rapidly. In the presence of STX, I_{Na} was not blocked for very short recovery times (50 ms), but then I_{Na} actually decreased as the "recovery" period was increased to 500 ms (i.e., block developed) until recovery from STX block eventually occurred at longer interpulse intervals. Short conditioning pulses are clearly necessary to elicit this post-repolarization development of block because it is not apparent with 5-s conditioning depolarizations (Fig. 4*B*).

A model for post-repolarization and phasic block

The results reported in Fig. 4*C* suggested binding to a conformation of the Na^+ channel that exists after repolarization; we therefore developed a model with three states, *R*, *B*, and *C* (Fig. 4*D*). *R* represents the state (or class of states) that the Na^+ channel assumes in equilibrium at −150 mV. *C* represents a conformation of the channel that exists transiently during the recovery process at −150 mV and has a high affinity for STX. *B* is the blocked toxin-bound state. Other kinetic states of the Na^+ channel, open (*O*) and inactivated (*I*) states, are included in the diagram as a suggested context, but they were not explicitly included in the model. It was assumed that during a depolarization the duration of the *C* conformation is very short and that after repolarization all channels come to state *C* with a time course that is rapid relative to STX binding. These simplifying assumptions are justified because nearly all I_{Na} had recovered from inactivation before STX block began to develop (Fig. 4*C, early points*). This also justified the use of a *C* state rather than an *I* state for the high-affinity state, because the high-affinity state for STX is one from which the channel can open upon depolarization. When the data for three STX concentrations (Fig. 4*C*) were fit individually to the three-state model (equations in the Appendix), the STX on rate (k_{CB}) was found to depend linearly upon the STX concentration, but the off rate (k_{BC}) and the channel gating rates (k_{CR} and k_{RC}) were very similar in the three concentrations. Thus the rate expected to depend upon STX concentration did depend upon it, and those not expected to depend upon it did not. We then fit the results for phasic block and for combined tonic and phasic block for all three concentrations simultaneously, and these

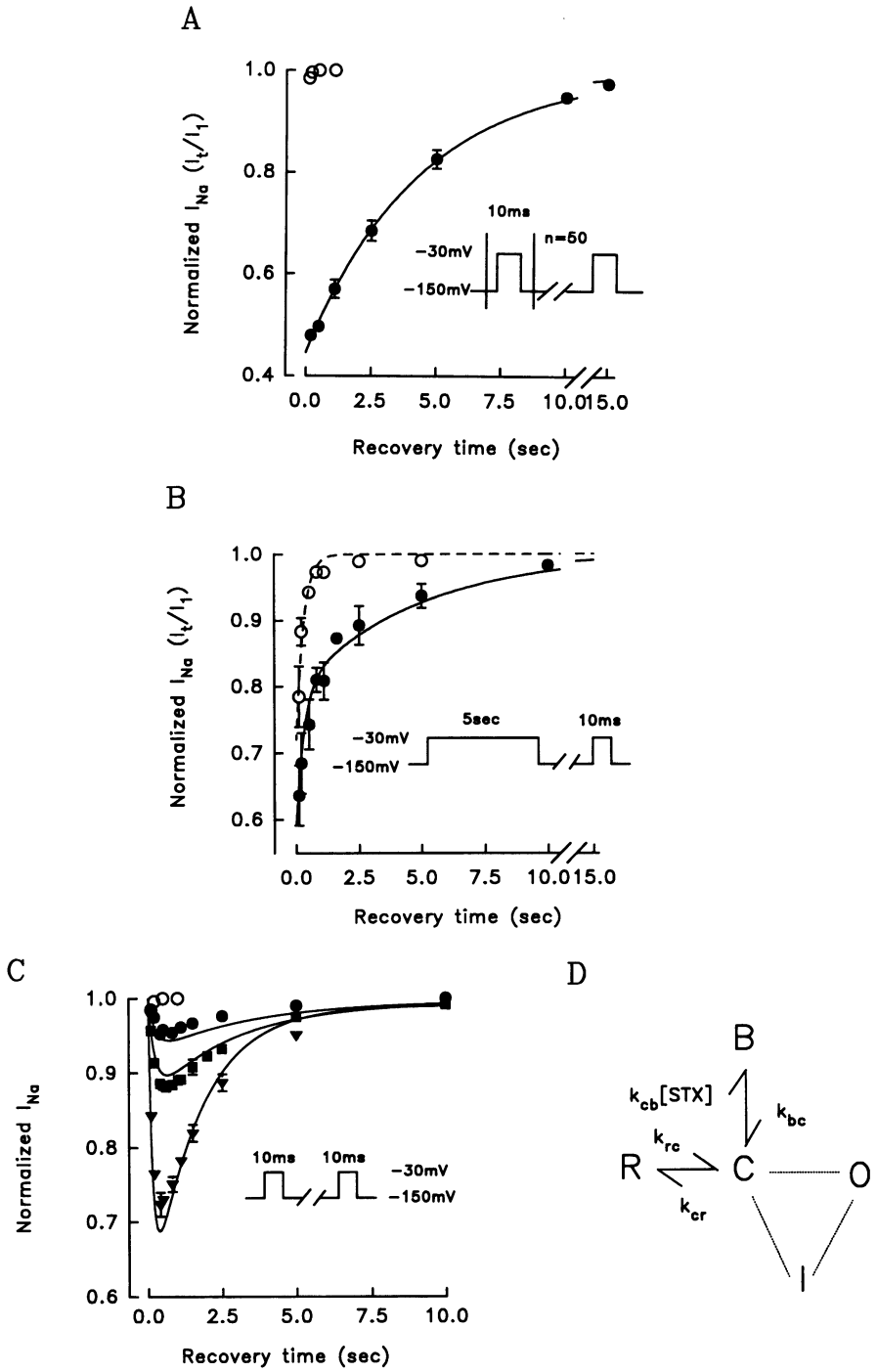

FIGURE 4 (*A*) Recovery from STX block induced by a train of 50 conditioning depolarizations to −30 mV from a holding potential −150 mV (see *inset*). I_{Na} elicited by a test pulse at various recovery times (I_t) was normalized to the I_{Na} elicited by the first pulse of the conditioning train (I_1). I_{Na} recovered rapidly in the absence of STX (○). I_{Na} recovered more slowly in 50 nM STX (●), τ = 4.3 ms as determined by a single exponential fit (——). The filled symbols represent mean ± SE from five determinations in two cells; for some points the SE bars are smaller than the symbols and are not displayed (fd.11, 13). (*B*) Recovery from STX block induced by a long conditioning depolarization (*inset*). The recovery time was defined by the interval between the conditioning pulse and the test pulse with current normalized as in *A*. In the absence of STX (○), I_{Na} at times greater than 100 ms recovered from inactivation as a single exponential (– – – –) with τ = 0.30 s and an amplitude of 0.28. In 50 nM STX (●) I_{Na} recovery was best fit by a two-exponential model with the more rapid component having a time constant τ_1 = 0.31 s and an amplitude of 0.21, and a slow component τ_2 = 4.9 s and an amplitude of 0.17. The STX data are represented as the mean ± SE from four cells (fd.13, 14, 20, 21). (*C*) Recovery from STX block induced by a single 10-ms conditioning depolarization. In control, recovery was rapid and complete by 100 ms (○). With STX (25 nM STX (●), 50 nM STX (■), 250 nM STX (▼)) I_{Na} first declined before recovery eventually occurred. The symbols and error bars represent the mean ± SE of data from two to four measurements. The solid lines are fits to the three-state model for post-repolarization block (Table 2, fit 3). (*D*) Diagram of a three-state model to account for the post-repolarization block by STX and subsequent recovery. *B*, STX bound state of the channel; *C* state of the channel with increased affinity for STX; *R*, ultimate rest state of the channel. Representations for the open state (*O*) and the inactivated states (*I*) are included for context but were not explicitly included in the model. k_{cb}, STX binding rate; k_{bc}, unbinding rate; k_{cr} and k_{rc}, transition rates of the channel not bound by STX.

rates are reported in Table 1. We first fit the model for the phasic block data only (Table 1, fit 1). Under this assumption, nonphasic block would occur through some other mechanism such as an affinity of STX for the *R* state. Two-pulse data were renormalized to control currents and were fit again to determine if the simple model could explain both phasic and first-pulse block (Table 2, fit 2). The model might account for nonphasic block through an equilibrium distribution between the *R*, *C*, and *B* states, allowing STX binding to the *C* state to occur at −150 mV. The resulting rate constants resulted in good fits to the two-pulse data (not shown). Although the model can account for nonphasic block, it does not exclude other mechanisms for nonphasic block such as binding to the *R* state.

To answer the question of whether or not the three-state model could also account for the block occurring in pulse trains, we derived a recurrence relation (see Appendix) based upon the three-state model to describe the expected block occurring in pulse trains. We assumed that no blocking or unblocking occurred during the 10 ms of the depolarization to −30 mV and that at the end of each depolarization, all channels not in state *B* were returned to state *C*. Rate con-

TABLE 1 Fits to three-state model for STX binding

Rates	Units	Description	Fit 1	Fit 2	Fit 3
k_{cb}	$s^{-1}\mu M^{-1}$	On rate	8.7 ± 1.4	14.3 ± .8	15.9 ± .4
k_{bc}	s^{-1}	STX off rate	0.78 ± 0.28	0.36 ± .05	0.19 ± .01
k_{rc}	s^{-1}	Gating kinetic	0.0006 ± 0.04	0.97 ± .06	0.88 ± .02
k_{cr}	s^{-1}	Gating kinetic	5 ± 1.1	1.34 ± .31	1.75 ± 0.8

Fit 1, 2-pulse phasic block only.
Fit 2, 2-pulse phasic block and first pulse block.
Fit 3, 2-pulse and pulse train phasic block and first pulse block ± approximate standard error of the parameter fit.

stants from a simultaneous fitting of the data in Figs. 3 and 4*C* are given in Table 1 (fit 3), and the solid lines in these figures represent the results of this fit. To improve presentation the data in Fig. 4*C* are normalized to the current in the conditioning step (I_1), but data were normalized to control currents (I_C) for this fit. The post-repolarization block model successfully described the concentration and frequency dependence of phasic STX block in two-pulse protocols (Fig. 4*C*); the fit of this model was better than the general guarded receptor model at rapid pulsing frequencies (Fig. 3).

DISCUSSION

Post-repolarization block has been reported previously for non-heart Na^+ channels using brief conditioning depolarizations (Salgado et al., 1986; Lönnendonker, 1989; Patton and Goldin, 1991). Post-repolarization block has not been described previously in heart, although a small amount of what might be post-repolarization block development can be observed for a 300-ms conditioning depolarization in Figure 6 of the study of TTX block by Cohen and co-workers (Cohen et al., 1981). The time course of post-repolarization block in heart (Fig. 4*C*) is more rapid than reported for non-cardiac preparations, occurring at about 0.5 s, whereas the peak of block development occurred at about 5 to 10 s for STX block in crayfish axons (Salgado et al., 1986), frog myelinated nerve (Lönnendonker, 1989), and rat brain II channels expressed in oocytes (Patton and Goldin, 1991). The rapid time course of post-repolarization block for cardiac I_{Na} is likely to be a consequence of the structures of the cardiac isoform because it has been demonstrated in studies of the rat heart I sodium channel expressed in oocytes (Satin et al., 1992b) that the rapid time course of post-repolarization block can be slowed by the same point mutation that increases TTX and STX sensitivity (Satin et al., 1992a).

The three-state model we propose is not intended as a comprehensive model of STX block of I_{Na} but rather as an explanation for post-repolarization block. The model has three essential features: (*a*) depolarization induces a conformational change in the channel, causing higher STX affinity, (*b*) this high-affinity conformation exists only transiently, and (*c*) the dwell time in the high-affinity state is governed by the "back" reaction (k_{CR}). STX binding to other states of the channel must be considered. As reported previously for TTX (Hille, 1968), STX had no effect on current time course (data not shown), as would be expected if it bound to and shortened the dwell time in the open state. Therefore, binding to the open state may be assumed to be small. STX binds to the inactivated state during a prolonged depolarization as in the conditioning pulse in Fig. 4*B* and as reported previously for TTX in heart (Cohen et al., 1981; Clarkson et al., 1988; Eickhorn et al., 1990), but the binding rates were on the order of seconds. Eickhorn et al. (1990) reported that 90% of phasic block developed during depolarizations as short as 1 ms, and we report that little additional block is produced by prolonging the duration of the depolarization to 50 ms. Therefore, binding to the inactivated state(s) is likely to be small for relatively short depolarizations. STX binding to the resting state is likely. Simulations with a four-state model that included STX binding to the *R* state, both with and without allowing transitions between the toxin bound states, showed that such a model could also fit the data, but the essential features of the three-state model were intact. Note that it is also necessary to postulate a trapping mechanism during depolarization for drug bound channels, that is, channels in the STX bound state (*B*) must gate to a state from which recovery is slow, otherwise complete recovery would be expected upon prolonged depolarization because the *C* state is vacated. Such gating among the toxin bound states must also exist because gating current appears not to be changed by TTX and STX (Armstrong and Bezanilla, 1974; Hanck et al., 1990).

The three-state model predicts the existence of a long-lived but transiently existing Na^+ channel conformation after a depolarization and during the recovery of I_{Na} with high affinity for STX. Although we show the STX binding model in the context of a simplified gating model (Fig. 4*D*), the exact relationship has not been defined. The conformational change that induces higher toxin affinity may be coupled to the gating process (as implied in Fig. 4*D*), or it may be independent of the gating process analogous to the way that activation and inactivation are independent in the Hodgkin-Huxley gating model. If not coupled, then the voltage-dependent transition to the high-affinity state would still provide a component of gating current. If coupled, then effects on channel gating properties such as latency to channel opening should also be affected.

Can a kinetic state lying between the inactivated state and the fully recovered state with the correct dwell time be found in reported kinetic models for the Na^+ channel? Most models do not include such a state. The Hodgkin-Huxley model (Hodgkin and Huxley, 1952) equilibrates rapidly to the resting state (*R*), providing dwell times of less than 1 ms in states along the way at −150 mV. A more recent and comprehensive

gating model for squid (Vandenberg and Bezanilla, 1991) also failed to yield such a state. A model for the cardiac Na^+ channel (Scanley et al., 1990) has a C state between open and rest at −150 mV with a dwell time of several hundred milliseconds. However, this model did not produce realistic recovery times (recovery data were not included in the fit), so this state may be fortuitous. Other cardiac models (e.g., Kunze et al., 1985), even those explicitly modeling recovery (Benndorf, 1989), did not report the rate constants at negative potentials required for this analysis. This property of toxin binding may therefore have implications for Na^+ channel gating, namely that equilibration to the ultimate resting state or states takes hundreds of milliseconds, a property not previously suspected from electrophysiological measurements. This predicts that latency to Na^+ channel opening, and therefore the decay rate of I_{Na}, might be different after brief depolarizations or after rapid pulse trains when channels might accumulate in this putative state and if this state is near the open state. Such a mechanism may account for the more rapid decay found in the I_{Na} traces after brief depolarizations (e.g., Frankenhaeuser, 1963; Baumann, 1981) in nerve or for the traces at the end of a rapid pulse train as compared with the first pulse in heart (Makielski and Falleroni, 1991).

The mechanism of post-repolarization block of I_{Na} may be a desirable property in an antiarrhythmic drug. Class III antiarrhythmic agents (Vaughan-Williams, 1984) prolong the action potential and secondarily tissue refractoriness. The antiarrhythmic effect is postulated to result from the prolongation of refractoriness, but action potential prolongation may predispose the patient to long-QT arrhythmias or Torsades des Pointes. A Na^+ channel-blocking drug having the property of post-repolarization block might have a beneficial effect on refractoriness without prolonging action potential duration, thus mitigating the potential negative effects of action potential slowing associated with other Na^+ channel-blocking drugs (Class I).

In summary, phasic block and post-repolarization block of cardiac Na^+ channels by STX can be accounted for by a model of block that postulates high-affinity STX binding to a conformational state of the Na^+ channel on the pathway of I_{Na} recovery after a depolarization. This model suggests a hitherto unsuspected conformation of the Na^+ channel, namely, at least one closed state during recovery that exists transiently for relatively long times even at very negative potentials.

APPENDIX

Guarded-receptor modeling

The guarded receptor model equations and terminology were adapted from Starmer (1988). Two equations were fit:

$$\lambda = t_a\lambda_a + t_r\lambda_r \qquad \text{Pulse train development rate (pulses}^{-1}\text{)} \qquad \text{(A1)}$$

$$a_{ss} = (a_\infty + \gamma(r_\infty - a_\infty))^*\beta \qquad \text{Steady-state phasic block} \qquad \text{(A2)}$$

where

$$\lambda_a = k_a[\text{STX}] + l_a \quad \text{and} \quad \lambda_r = k_r[\text{STX}] + l_r$$

$$a_\infty = (1 + l_a/[\text{STX}]k_r)^{-1} \qquad r_\infty = (1 + l_r/[\text{STX}]k_r)^{-1}$$

$$\beta = r_\infty/(1 - r_\infty) \qquad \gamma = (1 - e^{-\lambda_r t_r})/(1 - e^{-\lambda})$$

a_∞ is the amplitude of block at equilibrium binding of STX to the transient state, and r_∞ is the amplitude of "first-pulse" or "rest" block resulting from equilibrium binding to the resting state. Both a_∞ and r_∞ are normalized by dividing the amount of current in STX by the current in the absence of STX (control current). β is a conversion factor that takes the amplitude of phasic block normalized to the current from the first depolarization in the train and renormalizes it to control current. This allowed the model to fit data from the pulse trains only and reserved prediction of rest block as an independent verification of the model.

The three experimental variables are (a) [STX], the STX concentration (nM), (b) t_r, the interval between pulses in the train (seconds), and (c) t_a, the dwell time of the channel in the state during the depolarization to which STX binds with high affinity.

The four parameters of the guarded-receptor fit are (a) l_a, the off rate for the high-affinity state at −30 mV (s^{-1}); (b) k_a, the on rate for the high-affinity state at −30 mV ($s^{-1}nM^{-1}$); (c) l_r, the off rate for the resting state at −150 mV (s^{-1}); and (d) k_r, the on rate for the resting state at −150 mV (s^{-1}).

Equations A1 and A2 were fit using the SAS (Cary, NC) SYSNLIN nonlinear least-squares fitting procedure using the Gauss method with a CONVERGE criteria of 0.0001 running on a Sun Sparcstation SLC.

Assumptions used in the fit were that (a) phasic STX binding occurs predominantly to a transiently available state; (b) t_a was set arbitrarily to 1 ms, the l_a and k_a we report can be considered as reflecting the rates of interaction/millisecond of dwell time in the state, or in the case that more than one transient state is important in the binding, it is an averaged rate per ms dwell time in the states; (c) phasic block occurs after peak current is reached.

Post-repolarization block 3 state model

The three-state model with four rate constants depicted in Fig. 4*D* was used to describe the fractional occupancy of the channel in each of the states R, C, and B as a function of the time t: $R(t)$, $C(t)$, $B(t)$. Three differential equations were used to describe the dynamic process:

$$dR(t)/dt = k_{CR}C - k_{RC}R$$

$$dC(t)/dt = k_{BC}B + k_{RC}R - k_{CR}C - [\text{STX}]k_{CB}C$$

$$dB(t)/dt = [\text{STX}]k_{CB}C - k_{BC}B$$

where the rate constants account for STX binding (k_{CB}, $s^{-1}\mu M^{-1}$) and unbinding (k_{BC}, s^{-1}) and for the rates for entering (k_{RC}, s^{-1}) and leaving (k_{CR}, s^{-1}) the high-affinity state of the channel. The eigenvalues λ_1 and λ_2 for this system of equations are

$$\lambda_1 = (-k + b)/2$$

$$\lambda_2 = (-k - b)/2$$

where

$$c_w = \{R_0 - B_0(\lambda_2 + k_{BC})/([\text{STX}]k_{CB})\}\exp(\lambda_1 t)$$

$$c_x = \{B_0(\lambda_1 + k_{BC})/([\text{STX}]k_{CB}) - R_0\}\exp(\lambda_2 t)$$

$$c_y = [1 - \exp(\lambda_1 t)]/\lambda_1 - [1 - \exp(\lambda_2 t)]/\lambda_2$$

$$k = k_{RC} + k_{CR} + [\text{STX}]k_{CB} + k_{BC}$$

$$b = \{(k^2) - 4k_{RC}[\text{STX}]k_{CB} - 4k_{BC}(k_{RC} + k_{CR})\}^{1/2}$$

and R_0 and B_0 are the initial fractional occupancies in the R and B states, respectively ($R + B + C = 1$).

The analytic solution for the time course of fractional occupancy in the B state could then be expressed as

$$B(t) = [\text{STX}]k_{CB}(c_w + c_x)/(\lambda_1 - \lambda_2) + k_{RC}k_{CB}c_y/(\lambda_2 - \lambda_1) \qquad \text{(A3)}$$

The fraction of current remaining for the second pulse of the two-pulse experiments (Fig. 4*C*) was then assumed to represent the fraction of channels not blocked ($1 - B(t)$) at time t after the first pulse. The solution is not unique and depends upon the initial conditions. We used two different sets of initial values for the data normalized in two different ways. For fit 1 of Table 2, we assumed no initial occupancy in B, that is, we assumed the B state accounted for none of the rest block, and we normalized the data to be fit to the first pulse. For fits 2 and 3 of Table 2, we assumed an initial occupancy in state B, the value of which was obtained from the dose-response relationship for first pulse block. For these fits we normalized the data to control currents (in the absence of STX).

Equation A3 was fit to the data using the SAS (Cary, NC) NLIN nonlinear least-squares fitting procedure using the Gauss method with a CONVERGE criteria of 0.0001 running on a Sun Sparcstation SLC.

Recurrence relation for the block of peak I_{Na} in pulse trains

Let $P(n)$ be a function that describes the occupancy in the blocked state at the beginning of pulse n. An expression for P can be derived using the function for $B(t)$ (Eq. A3). The amount of block developed between pulse n and pulse $n - 1$ is given by $B(t_r)$, where B_0 in Eq. A3 can be considered the block associated with the previous pulse $P(n - 1)$. We also assume that after the pulse all channels not in B are in C, so that the R_0 term is zero. Inspection of Eq. A3 and c_w and c_x shows that B_0 is a linear term in the expression, therefore we can write

$$P(n) = aP(n - 1) + b \tag{A4}$$

where

$$a = (a_1 + a_2)/(\lambda_1 - \lambda_2)$$

$$b = b_1 + k_{RC}k_{CB}b_2/(\lambda_1 - \lambda_2)$$

$$a_1 = -(\lambda_2 + k_{CB} + k_{BC})\exp(\lambda_1 t_r)$$

$$a_2 = (\lambda_1 + k_{CB} + k_{BC})\exp(\lambda_2 t_r)$$

$$b_1 = [\exp(\lambda_1 t_r) - \exp(\lambda_2 t_r)]k_{CB}/(\lambda_1 - \lambda_2)$$

$$b_2 = [1 - \exp(\lambda_1 t_r)]/\lambda_1 - [1 - \exp(\lambda_2 t_r)]/\lambda_2$$

Listing explicitly the expressions for $P(n)$ where $n = 0, 1, 2, 3, \ldots$ will lead to a closed form solution for this linear homogeneous recurrence relation.

$$P(0) = B_0$$

$$P(1) = aB_0 + b$$

$$P(2) = a(aB_0 + b) + b = a^2B_0 + ab + b$$

$$P(3) = a(a^2B_0 + ab + b) + b = a^3B_0 + (a^2b + ab + b)$$

$$= a^3B_0 + b(a^2 + a + 1)$$

In general,

$$P(n) = a^nB_0 + b(a^{n-1} + a^{n-2} + \ldots + a^1 + 1).$$

The geometric series $a^{n-1} + a^{n-2} + \ldots + a^1 + 1 = (1 - a^n)/(1 - a)$ gives

$$P(n) = a^nB_0 + b(1 - a^n)/(1 - a) = [B_0 - b/(1 - a)]a^n + b/(1 - a).$$

This can be put into a natural log decay expression as

$$P(n) = [B_0 - b/(1 - a)]e^{\phi n} + b/(1 - a) \tag{A5}$$

where $\phi = \ln(a)$.

$P(n)$ therefore takes the form of a single exponential function with amplitude of phasic block represented by

$$a_{ss} = B_0 - b/(1 - a) \tag{A6}$$

and rate of development of block λ

$$\lambda = -\phi = -\mathrm{Ln}(a) \qquad (\mathrm{pulses}^{-1}). \tag{A7}$$

Equations A3, A6, and A7 were used to simultaneously fit $B(t)$ data (Fig. 4) from two-pulse protocols and the λ and phasic block (a_{ss}) data (Fig. 3) from pulse-train protocols to obtain fit 3 in Table 2. The SAS (Cary, NC) SYSNLIN nonlinear least-squares fitting procedure for systems of nonlinear equations was used for this fit.

Work on this study was supported by National Institutes of Health grant PO1 HL20592.

Dr. Makielski is an Established Investigator of the American Heart Association.

We thank David Piper for assistance in cell isolation, Dorothy Hanck for her data acquisition and analysis programs, and Daniel Chambers for help with mathematical modeling. We thank Harry Fozzard for helpful discussions and for his reading of the manuscript.

REFERENCES

Armstrong, C. M., and F. Bezanilla. 1974. Charge movement associated with the opening and closing of the activation gates of the Na channels. *J. Gen. Physiol.* 63:533–552.

Baer, M., P. M. Best, and H. Reuter. 1976. Voltage-dependent action of tetrodotoxin in mammalian cardiac muscle. *Nature (Lond.).* 263:344–345.

Baumann, G. 1981. Novel kinetics in the sodium conductance system predicted by the aggregation model of channel gating. *Biophys. J.* 35:699–705.

Benndorf, K. 1989. Patch clamp analysis of recovery of sodium channels from inactivation in mammalian myocardium in terms of a Markovian state model. *Biomed. Biochim. Acta.* 48:287–302.

Carmeliet, E. 1987. Voltage-dependent block by tetrodotoxin of the sodium channel in rabbit cardiac Purkinje fibers. *Biophys. J.* 51:109–114.

Clarkson, C. W., T. Matsubara, and L. M. Hondeghem. 1988. Evidence for voltage-dependent block of cardiac sodium channels by tetrodotoxin. *J. Mol. Cell. Cardiol.* 20:1119–1131.

Cohen, C. J., B. P. Bean, T. J. Colatsky, and R. W. Tsien. 1981. Tetrodotoxin block of sodium channels in rabbit Purkinje fibers: interactions between toxin binding and channel gating. *J. Gen. Physiol.* 78:383–411.

Courtney, K. R. 1975. Mechanism of frequency-dependent inhibition of sodium currents in frog myelinated nerve by the lidocaine derivative GEA 968. *J. Pharmacol. Exp. Ther.* 195:225–236.

Eickhorn, R., J. Weirich, D. Hornung, and H. Antoni. 1990. Use dependence of sodium current inhibition by tetrodotoxin in rat cardiac muscle: influence of channel state. *Pfluegers Arch. Eur. J. Physiol.* 416:398–405.

Fan, Z., and J. C. Makielski. 1992a. Block of cardiac Na^+ channels by STX suggests a long transient closed state associated with the post-depolarization period. *J. Physiol. (Lond.).* 459:170P.

Fan, Z., and J. C. Makielski. 1992b. Estimation of STX binding rates to cardiac Na channels. *Biophys. J.* 61(Part 2):A110.

Frankenhaeuser, B. 1963. Inactivation of the sodium-carrying mechanism in myelinated nerve fibres of *Xenopus laevis*. *J. Physiol. (Lond.).* 169: 445–451.

Gonoi, T., S. J. Sherman, and W. A. Catterall. 1985. Voltage clamp analysis of tetrodotoxin-sensitive and -insensitive sodium channels in rat muscle cells developing in vitro. *J. Neurosci.* 5:2599–2564.

Hanck, D. A., M. F. Sheets, and H. A. Fozzard. 1990. Gating currents associated with Na channels in canine cardiac Purkinje cells. *J. Gen. Physiol.* 95:439–457.

Hille, B. 1968. Pharmacological modifications of the sodium channels of frog nerve. *J. Gen. Physiol.* 51:199–219.

Hille, B. 1977. Local anesthetics: hydrophilic and hydrophobic pathways for the drug-receptor reaction. *J. Gen. Physiol.* 69:497–515.

Hodgkin, A. L., and A. F. Huxley. 1952. A quantitative description of membrane current and its application to conduction and excitation in nerve. *J. Physiol. (Lond.).* 117:500–544.

Hondeghem, L. M., and B. G. Katzung. 1977. Time- and voltage-dependent

interaction of antiarrhythmic drugs with cardiac sodium channels. *Biochim. Biophys. Acta.* 472:373–398.

Kunze, D. L., A. E. Lacerda, D. L. Wilson, and A. M. Brown. 1985. Cardiac Na currents and the inactivity, reopening, and waiting properties of single Na channels. *J. Gen. Physiol.* 86:697–719.

Lönnendonker, U. 1989. Use-dependent block of sodium channels in frog myelinated nerve by tetrodotoxin and saxitoxin at negative holding potentials. *Biochim. Biophys. Acta.* 985:153–160.

Lönnendonker, U. 1991. Use-dependent block with tetrodotoxin and saxitoxin at frog Ranvier nodes I. Intrinsic channel and toxin parameters. *Pfluegers Arch. Eur. J. Physiol.* 20:135–141.

Makielski, J. C., and M. J. Falleroni. 1991. Temperature dependence of sodium current block by lidocaine in cardiac Purkinje cells. *Am. J. Physiol.* 260:H681–H689.

Makielski, J. C., M. F. Sheets, D. A. Hanck, C. T. January, and H. A. Fozzard. 1987. Sodium current in voltage clamped internally perfused canine cardiac Purkinje cells. *Biophys. J.* 52:1–11.

Noda, M., H. Suzuki, S. Numa, and W. Stühmer. 1989. A single point mutation confers tetrodotoxin and saxitoxin insensitivity on the sodium channel-II. *FEBS Lett.* 259:213–216.

Patton, D. E., and A. L. Goldin. 1991. A voltage-dependent gating transition induces use-dependent block by tetrodotoxin of rat IIA sodium channels expressed in *Xenopus* oocytes. *Neuron.* 7:637–647.

Provencher, S. W. 1976. A Fourier method for the analysis of exponential decay curves. *Biophys. J.* 16:27–41.

Salgado, V. L., J. Z. Yeh, and T. Narahashi. 1986. Use- and voltage-dependent block of the sodium channel by saxitoxin. *In* Tetrodotoxin, Saxitoxin and the Molecular Biology of the Sodium Channel. Vol. 479. C. Y. Kao and S. R. Levinson, editors. New York Academy of Sciences, New York. 84–95.

Satin, J., J. W. Kyle, M. Chen, P. Bell, L. L. Cribbs, H. A. Fozzard, and R. B. Rogart. 1992a. A mutant of TTX-resistant cardiac sodium channels with TTX-sensitive properties. *Science (Washington DC).* 256:1202–1205.

Satin, J., J. W. Kyle, R. Rogart, H. A. Fozzard, and J. Makielski. 1992b. Phasic STX block of I_{Na} is altered by point mutations of the cloned cardiac Na channel expressed in *Xenopus* oocytes. *J. Mol. Cell. Cardiol.* 24:S36a.

Scanley, B. E., D. A. Hanck, T. Chay, and H. A. Fozzard. 1990. Kinetic analysis of single sodium channels from canine cardiac Purkinje cells. *J. Gen. Physiol.* 95:411–435.

Starmer, C. F. 1988. Characterizing activity-dependent processes with a piece-wise exponential model. *Biometrics.* 44:549–559.

Starmer, C. F., and A. O. Grant. 1985. Phasic ion channel blockade: a kinetic model and parameter estimation procedure. *Mol. Pharmacol.* 28:348–356.

Starmer, C. F., A. O. Grant, and H. C. Strauss. 1984. Mechanisms of use-dependent block of sodium channels in excitable membranes by local anaesthetics. *Biophys. J.* 46:15–27.

Ulbricht, W., H. H. Wagner, and J. Schmidtmayer. 1986. Kinetics of TTX-STX block of sodium channels. *In* Tetrodotoxin, Saxitoxin and the Molecular Biology of the Sodium Channel. Vol. 479. C. Y. Kao and S. R. Levinson, editors. New York Academy of Sciences, New York. 68–83.

Vandenberg, C. A., and F. Bezanilla. 1991. A sodium channel gating model based on single channel, macroscopic ionic, and gating currents in the squid giant axon. *Biophys. J.* 60:1511–1533.

Vassilev, P. M., R. W. Hadley, K. S. Lee, and J. R. Hume. 1986. Voltage-dependent action of tetrodotoxin in mammalian cardiac myocytes. *Am. J. Physiol.* 251:H475-H480.

Vaughan-Williams, E. M. 1984. A classification of antiarrhythmic actions reassessed after a decade of new drugs. *J. Clin. Pharmacol.* 24:129–135.

Watanabe, T., and T. F. McDonald. 1986. Tetrodotoxin exerts a large frequency-dependent depression of the maximum rate of rise of action potentials in guinea pig ventricular myocytes. *Pfluegers Arch. Eur. J. Physiol.* 406:645–647.